Scale and Temperature Dependent Creep Modeling and Experiments in Materials

Ming Gan and Vikas Tomar

Creep is non-recoverable high temperature plastic deformation occurring at low load regimes, constant stress values, and small strain rates. While mechanistic information regarding macroscale (centimeters and higher) creep deformation has been of significant attention in the past few decades, the nanoscale (few nanometers to a few hundred nanometers) and microscale (few hundred nanometers to a few hundred micrometers) creep deformation has recently emerged as an important area of research. A particular interest lies in trying to control nanoscale and microscale creep properties with a view to design materials for extreme environments and materials in small scale devices. This article presents an overview of the recent developments in modeling and experiments focused on analyzing nanoscale and microscale temperature dependent creep in materials.

INTRODUCTION

Creep is non-recoverable high temperature plastic deformation occurring at low load regimes, constant stress, and small strain rates. Creep occurs in the form of transient deformation of a material leading to permanent plastic strain at applied stress values lower than the material yield stress. Characterization of creep deformation is especially considered important in the case of materials intended for use at high temperatures. Creep of bulk materials starts with a decreasing strain rate in the primary (initial) stage followed by a steady state—the secondary stage creep. After that, in the tertiary stage, the strain rate increases again until the materials fails. Being a transient deformation, creep strain rate is the most critical defining parameter of a material's creep strength. Usually the most critical creep strain rate is the steady state strain rate in the secondary stage, when the generation and the recovery of dislocations compensate each other.[1] This is also usually the minimum strain rate in the creep strain rate vs. stress curve. It always increases with temperature, and it becomes severe when the temperature approaches the melting point of the material. Creep response of a material has been shown to be affected by varied parameters such as material's elastic property values, measurement temperature, loading rate, creep time, maximum load, as well as average grain size in the case of polycrystalline materials. The creep curves are usually described in the form Norton power law relationship between the strain rate $\dot{\varepsilon}$ and stress σ as,[2]

$$\dot{\varepsilon} = A\sigma^{n} exp\left(-Q / RT\right) \qquad (1)$$

Here, A is a material coefficient, n is referred to as stress exponent, Q is thermal activation energy of a material, R is universal gas constant, and T is measurement temperature. The relationship is particularly shown to be valid when the temperature is higher than 0.5 times the melting temperature (T_m). This relationship inherently assumes that deformation mechanism is thermally activated. This may not be true if the creep occurs under high stress values.

The stress exponent n in Equation 1 is considered as an indicator of creep mechanism. The n value is usually obtained by plotting the $\dot{\varepsilon}$ vs. σ curve in Equation 1 in double-log coordinates, where n will be the slope of the curve. The stress exponent n equals to 1 in the case of Coble creep.[3] Coble creep is thought to be controlled by diffusion of vacancies along the grain boundaries in nanocrystalline materials. Similar

How would you…

…describe the overall significance of this paper?

Characterization of creep deformation is important in materials uses at high temperatures. Such deformation occurs when the temperature of operation is much lower than the melting point. Creep deformation in this case occurs at nanoscale contacts at moderate temperatures much lower than the melting point of a material. Characterization of such nanoscale creep deformation is important for applications related to operation of miniature devices, thermal stability of interfaces etc. This article presents an overview of advances in this area.

…describe this work to a materials science and engineering professional with no experience in your technical specialty?

Creep occurs in the form of transient deformation of a material leading to permanent plastic strain at applied stress values lower than the material yield stress. During nanoscale or microscale indentation tests contact stresses are high. Nominal pressure during nano- and microindentation can reach a few percent of the Young's modulus; as a result, applied stress may approach ideal strength of a material. Due to such high stress contacts indentation creep can occur at low homologous temperatures even though the same material would not exhibit any creep under bulk conditions at the same temperature.

…describe this work to a layperson?

Nanoscale and microscale creep deformation has recently emerged as an important area of research. A particular interest lies in trying to control nanoscale and microscale creep properties with a view to design materials for extreme environments and materials in small scale devices. This article presents recent developments in modeling and experiments focused on analyzing nanoscale and microscale temperature dependent creep in materials.

to the Coble creep, the stress exponent is also 1 for Nabarro–Herring creep, which is thought to be controlled by diffusion of vacancies through the grains.[4] When exponent n is equal to 2, it is usually believed that the creep mechanism is dominated by grain boundary sliding.[5] Harper and Dorn have shown a creep mechanism named after them when they investigated the creep behavior of polycrystalline aluminum.[6] The measuring temperature in their experiments was close to the melting point of aluminum. They claimed that the Harper–Dorn creep occurs through a dislocation climb mechanism, where the creep rate increases in proportion to the fourth power of the stress. This mechanism has been one of the most contentious creep mechanisms. Langdon contended that this mechanism doesn't exist in reality.[5] Exponent n equals to 3 is the case where the creep is mainly because of diffusion-controlled dislocation movement including both the generation and the annihilation.[7,8] In this case, the density of dislocations varies approximately in proportion to the square of normal stress σ normalized by the shear stress $\mu(T)$. However, Kassner et al.[9] insisted that n should be 5 for this case. Another five-power-law model was raised by Sherby and Burke in 1968,[10] based on climb-controlled dislocation motion instead of dislocation and vacancy diffusion driven creep.

An important instance of creep deformation occurs when the temperature of operation is much lower than the melting point. Creep deformation in this case occurs at nanoscale contacts at moderate temperatures much lower than the melting point of a material. Characterization of such nanoscale creep deformation is important for applications related to the operation of miniature devices, thermal stability of interfaces, etc. Such knowledge can also be important for developing and designing materials in other types of extreme environments such as nuclear environments. The creep test at the nanoscale can be conducted by holding the indenter in a nanoindentation test at the maximum load and by monitoring subsequent indenting depth as a function of time. Indentation creep is usually monitored based on continuous indenter displacement when the indentation load is held at a constant value. Indentation creep experiments with typical holding times of 500 seconds have been used to characterize such creep deformation.[11] Fundamentally, during nanoscale or microscale indentation tests contact stresses are high. Correspondingly, nominal pressure during nano- and microindentation can easily reach a few percent of the Young's modulus of materials resulting in a situation where applied stress may approach ideal strength of a material. Due to such high stress contacts indentation creep can occur at low homologous temperatures (T/T_m) even though the same material would not exhibit any creep under bulk conditions at the same temperature.

NANOINDENTATION CREEP

Combined with the indentation technique, creep test can be conducted on thin films and coatings besides bulk specimens. Furthermore, indentation creep can be used to investigate the creep behavior of high-melting-point materials at room temperature, as bulk creep usually does not happen to these materials at low temperature. For high-melting-point materials, plasticity should serve as a prerequisite condition for creep to happen.[12,13] Most materials, including ceramics, exhibit indentation creep at temperatures down to 300 K due to high stresses involved in the indentation creep.[11] Unlike the creep curve from tensile creep tests, the one from indentation creep tests does not show the tertiary creep stage. The strain rate decreases in the initiation stage and reaches a constant value in the secondary stage. Thereafter, the strain rate remains constant till failure.

Nanoindentation creep has been observed in a wide range of materials including glasses, ceramics, and metallic materials.[11, 14,15] The indentation creep rate for high-melting-point materials can be of the order of 5×10^{-5} s^{-1}. This is a large value when compared to the corresponding bulk strain rate. The models for indentation creep are the same as those for bulk creep, with the equivalent stress exponent, n, used as an indicator of the creep mechanism.[11] However, during indentation creep tests on certain metals, alloys, and ceramics at room temperature, high n values up to hundreds have been observed.[12,13,15–19] Such n values are obtained when it is assumed that the Norton power law relationship is still applicable. Due to the lack of an observation tool, mechanistic explanation and modeling of such behavior has been difficult. It is possible that a power law based relationship may not be applicable in its entirety. The mechanism behind such high stress exponent values has often been attributed to volumetric densification and dislocation pile up. Materials systems analyzed include metallic thin films, e.g. Cu, Al, Ni,[20–223] thin films made of metallic alloys, e.g. Ni_3Al,[23] and ceramics e.g. ZrO_2,[24] and SiC-based.[25–27] During such studies, the size of the indenter (owing to indentation size effect—ISE) and the grain size of the polycrystalline materials have been shown to strongly affect the indentation creep response of materials. Besides the ISE and the grain size effect, the creep deformation mechanism is also shown to be affected by the test temperatures and the change in microstructure of the material as a result of temperature change. It has also been shown that fiber reinforcement,[28] or particle reinforcement,[29] can constrain creep rate.

Indentation Creep Models

Various mechanisms of bulk tensile creep are still considered valid in the case of indentation creep, with the stress exponent n used as an indicator of deformation mechanism. However, the method to derive the stress exponent is different, as the stress σ and strain rate $\dot{\varepsilon}$ can not be measured directly during the indentation creep tests. For the power law relationship between creep rate and equivalent stress, Ma and Yoshida[30] used a model given as,

$$\sigma = b\dot{\varepsilon}^m \qquad (2)$$

Here b and m are material constants. There are several models to derive the stress exponent for indentation creep, based on the relationship among creep depth (h), load (P), and time (t). These models are also indenter-related.[31] For pyramidal indenters, the most widely used relationship is the derivation of creep rate from indentation depth, depth changing rate with respect to

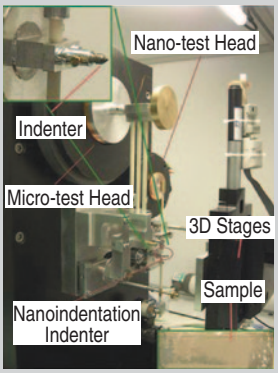

a

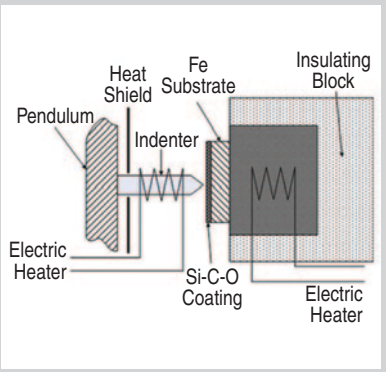

b

Figure 1. Experimental setup. (a) The setup of nano- and microscale testing heads and (b) schematic of the high temperature indentation approach.

time, and equivalent stress from applied load and contact area as[18,19,32]

$$\dot{\varepsilon} = \frac{1}{h}\frac{dh}{dt} \quad (3)$$

and

$$\sigma = \frac{P}{A_c} \quad (4)$$

In Equation 3, A_c is the contact area. The creep rate can be derived by differentiating the measured creep curve (h vs. t). The stress σ is derived from the maximum load P and corresponding contact area A_c. Li et al.[11] claimed that the principle mechanism causing indentation creep is dislocation glide plasticity in the temperature range from 300 K to the melting point. But when the grain size is less than 0.3–0.4 μm, indentation creep may be dominated by grain boundary diffusive creep (Coble creep). The loading rate has a considerable effect on the creep behavior of polymeric and solder alloy materials. The creep depth increases with the loading rate for PMMA[33] and a solder alloy,[30] which means a higher loading rate leads to a higher creep strain rate. For the solder alloy, the higher loading rate also results in a shallower penetration depth, thus higher indentation hardness.[30] The holding time at the maximum load also affects the creep curve significantly. Experiments have shown that both the measured elastic modulus and hardness decrease with the holding time for PMMA.[33]

Size Effect

Indentation size effect (ISE) commonly refers to the size dependence of strain rate sensitivity of materials in the case of self-similar indentation. Higher strain rate sensitivity at smaller indentation size in the case of self-similar indentations is referred to as positive strain rate sensitivity. Some materials also exhibit negative strain rate sensitivity, whereas reduction in strain rate sensitivity is observed at smaller indentation sizes. For an indentation with Berkovich indenter to be self-similar, the indentation depth should be larger than an indenter radius related value[15,34] given as

$$R_i\left(1 - sin70.3^o\right) \approx 0.06\,R_i \quad (5)$$

Creep results of nano-crystalline Cu, W, Al, and Ni indicate that both hardness and creep strain rate have shown a remarkable positive ISE.[21,22,35] Nanocrystalline and single-crystalline Ni_3Al also shows positive ISE.[23] It has been suggested that in the case of nano-crystalline Ni_3Al and Al, as the indentation size increases the creep mechanism changes from linear diffusion flow to a power-law mechanism, such as climb, and eventually to a rate-insensitive plastic flow.[15] Fused silica shows minor ISE. That is why it is usually used as a reference sample for indentation tests.[36] Negative strain rate sensitivity has been observed in some nanostructured and conventional aluminum alloys.[37,38] It is believed that such effect is caused by a small scale phenomenon known as Portevin–LeChatelier phenomenon associated with interactions between dislocations and solutes.[39] ISE can be affected by grain boundaries. It is suggested that the high volume fractions of grain boundary or triple junctions and the lower density of geometrically necessary dislocation in a nano-crystalline metal can weaken ISE.[40] The surface contamination might also account for the ISE in some cases.

Pop-in

During nanoindentation creep measurements, a pop-in occurs in the form of constant load displacement in load-displacement curve at a critical load during a load ramp. If the peak load is below the critical pop-in load, the deformation is purely elastic, except for very long holding time at loads slightly lower than the pop-in load where a delayed type of pop-in may occur.[41] This further implies that plasticity is a prerequisite for indentation creep.[12,15] However, such pop-in load is not observed for amorphous fused silica and most other ceramics.[18] For some low-melting metals, such as indium, creep can happen even before pop-in.[12]

CREEP SIMULATIONS

Finite element (FE) method is usually a method of choice to analyze creep behavior of materials. FE simulations are usually carried out using commercial software, e.g. ABAQUS, with user defined functions and parameters.[42–44] Such models assume that strain in the second stage of creep obeys the Norton's creep law or a similar power law with non-dimensional factors, length scale dependent factors included. The results show that the indentation creep behavior depends on the geometric fea-

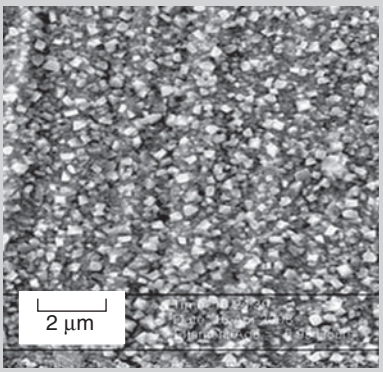

a

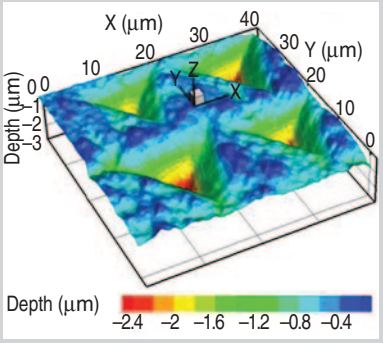

b

Figure 2. (a) SEM images of Si-C-O ceramic coatings and (b) image showing a comparison of the indentation depth with the Si-O-C coating surface.

tures of the system being analyzed, e.g. particle dimensions, indenter size, and thickness as well as on the creep properties of all components in the system.[42] Significant advances in simulations are needed to address microstructure dependent creep behavior of different materials.

TEMPERATURE DEPENDENT NANOINDENTATION CREEP

Recently, Gan and Tomar[45] for the first time presented nanoindentation and microindentation creep analyses on a material at temperatures ranging from room temperature to 500°C. The material system of focus was Si-C-O polymer derived ceramic coatings (PDC) made using polymer-precursor processing. Low creep rate is an essential property of this material system. Grain boundaries are not present in this material system. Possible length scale related factors influencing creep rate include phase transformation, change in porosity, etc. Nano- and micro-scale investigations of creep deformation can provide important insights into achieving control of creep in this material system. While nanoindentation can give information about features such as individual particles, microindentation can reveal information about the mechanical behavior of collective microstructural features over a larger area.

The coating thickness is approximately 15 μm. All tests were performed using a multi-module mechanical tester (Micro Materials Ltd., U.K.) shown in Figure 1. Figure 1b illustrates the setup for performing high temperature indentation. Both the sample and the indenter tip were heated to the required testing temperature which was closely monitored using thermocouples. The remaining parts of the setup, which have to be maintained at room temperature, are separated using heat shields. The tests were performed at 6 different temperatures: room temperature, 100°C, 200°C, 300°C, 400°C, and 500°C. The tip radius of the nanoindenter is approximately 20 nm and that of the microindenter is approximately 200 nm. Both indenters are of the Berkovich type. During the tests, the samples were mounted on the indentation stage using glue. The indenter approached the sample in its thickness direction,

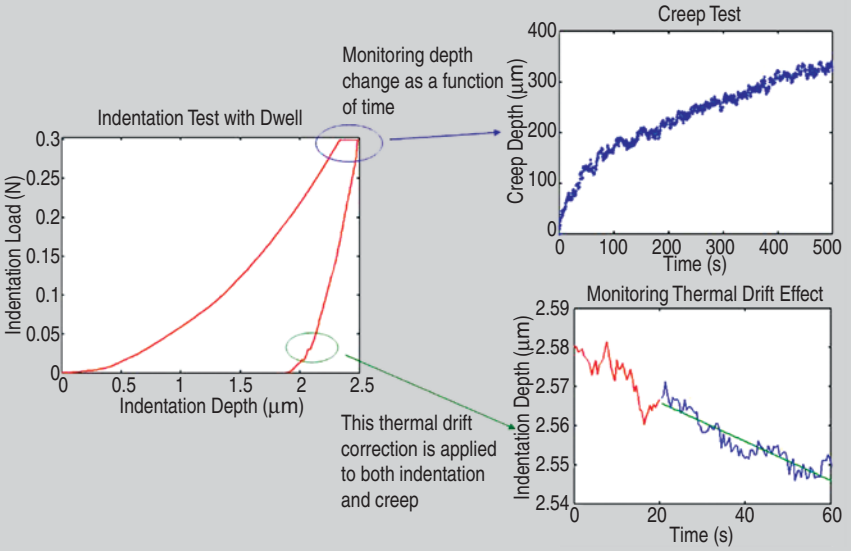

Figure 3. A typical nanoindentation profile showing how the creep data is extracted and how the thermal drift rate is extracted.

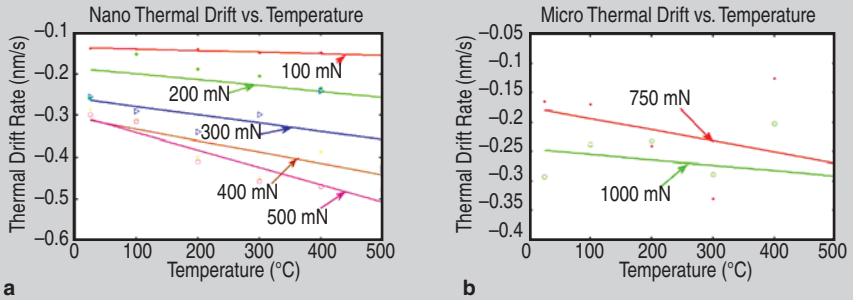

Figure 4. Thermal drift rate as a function of temperature and the peak indentation load in the case of (a) nanoindentation and (b) microindentation.

Figure 1b. Indentation locations were selected randomly on sample surfaces. In the case of each chosen location, tests were performed in either a 3 by 3 matrix or in a 4 by 4 matrix pattern with equal longitudinal and transverse spacing between each indentation spot of approximately 5 μm in the case of nanoindentation and 20 μm in the case of microindentation. The indentation depths and maximum indentation load were chosen to minimize the effect of measurement drift that usually occurs in indentation tests if the depth is too small.

Figure 2 also shows a surface scan of a coating after microindentation test at the peak indentation load of 750 mN. As shown, the microindentation depth is significantly larger than the size of surface asperities. Therefore, the surface roughness does not affect the microindentation test results. Since the length scale of nanoindentation tests is of the order of the size of particles, the surface roughness also does not affect nanoindentation results. Before starting the indentation tests, efforts were made to minimize the effects of thermal drift by allowing thermal equilibrium to be reached. This was ensured by setting the experimental setup idle for 2 hours at each temperature before each indentation testing run. The whole testing system was kept in a chamber to keep the temperature constant, which was set to be 3 degrees above the environmental temperature. A Berkovich diamond indenter was used in this experiment, for which the contact area as a function of indenting depth was calibrated using fused silica and tungsten reference samples at room temperature.

Figure 3 shows an example of the procedure used to extract the indentation creep data. The creep deformation profile is extracted from the dwell period at the peak load, Figure 3. Dwell period may affect the creep data. A number of dwell periods were tried. A dwell period of 500 s was decided based on convergence in the measurements. Indentation profiles were imaged before and after the tests to ensure that simi-

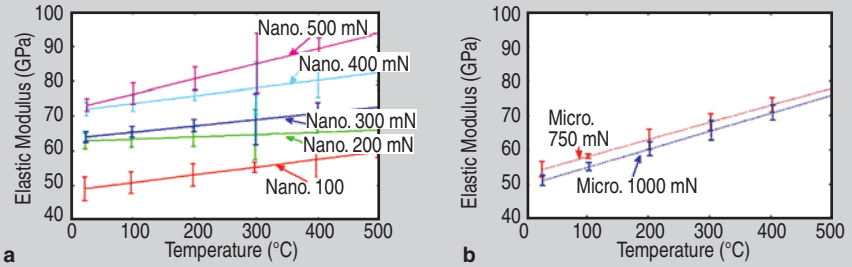

Figure 5. (a) Nanoindentation elastic moduli and (b) microindentation elastic moduli of Si-C-O coatings as a function of temperature and maximum indentation load.

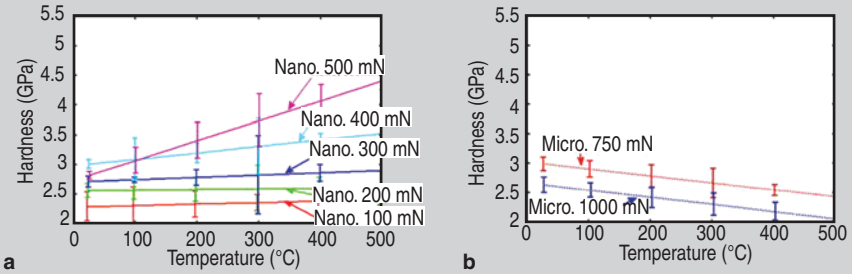

Figure 6. (a) Nanoindentation hardness and (b) microindentation hardness of Si-C-O coatings as a function of temperature and maximum indentation load.

lar surface conditions exist before and after the tests. At each load, more than nine independent indentations were performed.

One major concern is the stability of the indentation equipment as measurement temperature is increased. As a result of changes in stability, the measured depth as a function of time may drift from the actual value. Such a drift is sometimes referred to as thermal drift. During experiments, care is taken to minimize thermal drift by allowing thermal equilibrium to be reached. In addition, thermal drift rate is measured during each indentation test to adjust the measured data. In order to measure thermal drift rate for each indentation run, the indentation load was held constant for a period of 100 s typically at 10% of the peak during unloading, Figure 3. Figure 4 shows the averages of measured thermal drift rates as a function of peak indentation load and temperatures during nanoindentation and microindentation tests. As shown, thermal drift rate is a strong function of the peak indentation load at both length scales. The thermal drift rate increases with an increase in load and temperature at both scales. The magnitude of thermal drift rate is higher at the nanoscale owing to much higher sensitivity of measurements at the nanoscale. During calculation of creep data, the thermal drift rate is multiplied by the dwell time and then the result is subtracted from the measurement.

During analyses, the temperature dependent (from room temperature up to 500°C) nanoscale and microscale elastic moduli of the Si-C-O coating were first measured. The maximum load in the nanoindentation creep tests varied from 100 mN to 500 mN, with an increment of 100 mN. For the microindentation creep tests, the maximum loads were 750 mN and 1000 mN. The unloading rate was set to be 10 mN/s ~ 20 mN/s, depending on the peak load. Load and depth calibration were performed before each experiment for better precision of the measurement.

Analyses Results

After correcting for both creep and thermal drift, Figure 5 shows the elastic moduli values as a function of testing temperature and peak indentation load. As shown, the elastic moduli increase with increase in temperature and with increase in peak load at the nanoscale. At the microscale the elastic moduli increase as a function of temperature. However, dependence on the peak load at the microscale is not clear. Increase as a function of peak load signifies the ISE. It has been shown that Young's modulus of SiO_2 will increase with temperature due to compaction and distortion of SiO_4 tetrahedra in the temperature range of experiments. The underlying SiCO matrix retains this attribute. An examination of Figure 5a reveals the ISE is stronger at higher temperatures. The ISE is absent in the case of microscale data. The reason behind the observation of ISE at the nanoscale is not clear. For each data point in Figure 5a, a minimum of 16 tests were performed. Therefore a possibility that a single microstructural aberration is contributing to the ISE is ruled out. At the nanoscale the nanoindenter radius is approximately 20 nm and projected area is approximately 0.5 μm^2. Accordingly, the indenter samples either the SiC particles or small spaces of SiCO matrix between adjacent $TiSi_2$ particles. The ISE, therefore, can be attributed to increasing nanoscale densification with increasing indentation depth. At the microscale collective deformation of a sample volume containing many SiC particles takes place. Due to such collective motion of particles under indenter tip, the effect of volumetric densification under indenter tip is minimized leading to the absence of ISE. Increase in temperature contributes to increased binding of $TiSi_2$-SiCO interfaces invariably leading to increase in the elastic moduli values as a function of temperature at both scales.

Figure 6 plots the hardness data corresponding to the moduli plots in Figure 5. As shown, at the nanoscale the trend for the elastic moduli is repeated for the hardness values. A clear trend on increase in Meyer's exponent with increase in temperature emerges from nanoindentation data. The microindentation hardness data trend is opposite to the trend shown in the case of microindentation elastic moduli. Hardness decreases as the measurement temperature increases. In addition, hardness reduces with increase in the peak indentation load, signifying strain softening of the material. Reduction of hardness with increase in temperature is attributable to stronger $TiSi_2$ particles pressing in relatively softer SiCO matrix getting progressively softer with an increase in temperature at the microscale. At the nanoscale not enough contact area is available to have such an effect. Data on correlation between temperature-dependent hardness and Young's moduli values for ceramics is not available in the literature. A similar trend (increase in moduli and decrease in hard-

ness as a function of temperature) has been observed for chromium steels by Medved and Bryukhanov.[46]

It has been shown that in Si-C-O PDCs in amorphous phase the deformation during indentation occurs due to volumetric densification events. It has been shown that volumetric densification promotes strain hardening in vitreous silica under both indentation and diamond-anvil compression experiments.[27] The microindentation experiments on the present materials in the amorphous state reveal a reduction of indentation hardness under increasing applied loads, indicating densification-assisted strain softening of these materials.[27] A combination of nanoscale and microscale results points that individually neither the SiCO matrix nor $TiSi_2$ particles show strain softening. However, mechanistic effects related to their combined presence at the microscale results in strain softening behavior. Cheng and Cheng,[47] have pointed out that indentation hardness is not a function of indentation depth for materials that truly follow power-law strain hardening.

This is in contrast to the nanoindentation and microindentation results from the present materials that show an increase in hardness with increasing load during nanoindentation and reduction in hardness with increasing load during microindentation. Apart from the influence of strain hardening or softening, material pile-up around the indent and indentation creep can also contribute to indentation hardness behavior observed in the present work.

Figure 7 plots creep depth as a function of dwell period at three different temperatures at two different nanoindentation and microindentation peak loads. Creep data is normalized by subtracting the initial depth of each creep test. For comparison, the plots also show the thermal drift uncorrected as well as corrected data. As expected, the effect of thermal drift correction is the highest at the highest temperature and at the nanoscale. The creep depth vs. time plots reached steady state within first 100 s of plotting in all cases. Effect of temperature is to increase the creep rate. The temperature effect is more pronounced at the micro-scale in comparison to the nanoscale. The trend is particularly strong when transitioning from 250°C to 500°C.

Figure 8 plots stress exponent and creep strain rate as a function of temperature and peak indentation load at both length scales. Stress exponent at the nanoscale lies in the range of 4 to 5 indicating a dislocation climb related creep deformation mechanism occurring through bulk or pipeline diffusion of dislocations. The exponent reduces with an increase in temperature indicating a transition of mechanism from dislocation climb to diffusion. The densely dislocated structure with high dislocation density under indenter may result in dense dislocation channels directing atoms from dislocated cores to free surfaces resulting in such a mechanism occurring at low homologous

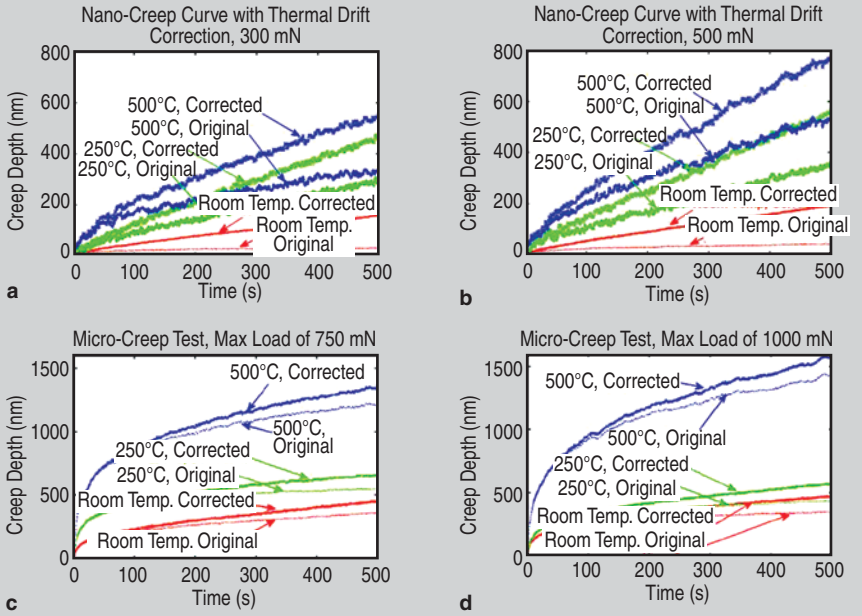

Figure 7. Indentation depth (original and thermal drift corrected) as a function of time at different temperatures in the case of (a) nanoindentation test at the peak load of 300 mN, (b) nanoindentation test at the peak load of 500 mN, (c) microindentation test at the peak load of 750 mN, and (d) microindentation test at the peak load of 1000 mN.

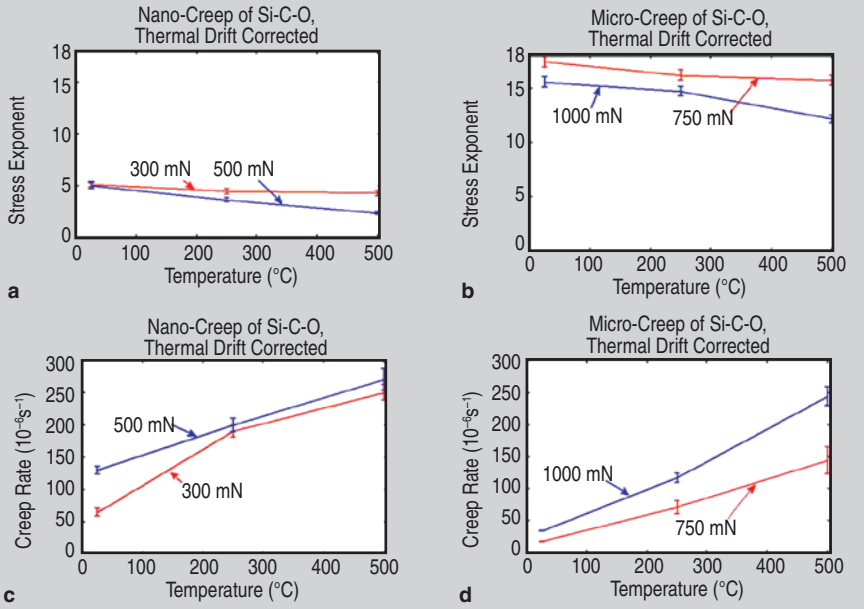

Figure 8. (a) Stress exponent as a function of load during nanoindentation creep measurements, (b) stress exponent as a function of load during microindentation creep measurements, (c) creep strain rate as a function of load during nanoindentation creep measurements, and (d) creep strain rate as a function of load during microindentation creep measurements.

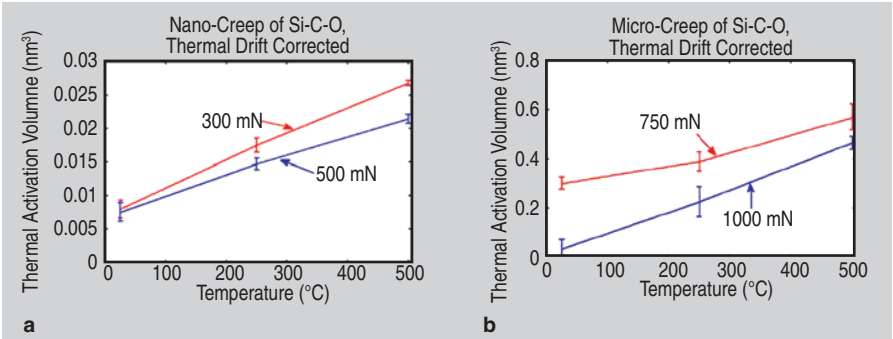

Figure 9. Thermal activation volume as a function of peak indentation load and measurement temperature at (a) nanoscale and (b) microscale.

temperatures. At the microscale the stress exponent is considerably higher indicating that primary mechanism of deformation is volumetric densification. Such a transition suggests a rapid change of mechanism from linear diffusion flow to power law mechanism (e.g. climb) and eventually to rate insensitive plastic flow (dislocation glide) as the indentation size moves towards microscale regime. The disparity in stress exponent values at the two length scales is not reflected in the creep strain rate data. As shown, the creep strain rates at both length scales lie in the same range with microscale data being on the lower side. Creep strain rate generally increases as a function of increase in temperature as well as with increase in peak indentation load. The creep strain rate at the microscale being lower than that at the nanoscale can be attributed to the averaging effect of measurements. As discussed earlier, in the case of microscale measurements, the indenter covers an area that is approximately 10 times larger than the nanoindenter area. Since hardness reduces and creep strain rate increases with increase in temperature at the microscale, the strain rate sensitivity index (constant k in relation $\sigma=b\,\dot{\varepsilon}^{k}$) indicates strain softening at the microscale. The same analyses reveal strain hardening at the nanoscale.

MODEL BASED ANALYSES

In general, in the case of PDCs both dislocation dominated and volumetric densifying type of deformation mechanisms with varying degree are present during indentation. In the case of quartz, the size effect on the stress exponent can be explained by a reduction of the localized shear volume as the indent size decreases. However, in the present work the size effect is related to shift from dislocation climb and diffusion related mechanism at the nanoscale to volumetric densification at the microscale (Figure 8). The extent of a particular type of mechanism determining deformation is governed by the availability of excess free volume which is related to thermal activation volume, which is also the average change in volume of the flow unit. Low-temperature creep deformation strain rate, $\dot{\varepsilon}$, of materials can be expressed by Arrhenius-type flow function,[48]

$$\dot{\varepsilon} = \dot{\varepsilon}_o \exp\left[-\frac{\Delta G(\sigma)}{k_B T}\right] \qquad (6)$$

In the above equation, $\dot{\varepsilon}_o$ is reference strain rate that varies with the type of material, stress level, and microstructure, ΔG is the activation energy for creep or other rate-dependent process, k_n is Boltzmann's constant, and T is temperature in Kelvin. Parameter $\dot{\varepsilon}_o$ is proportional to the concentration of elementary defects which cause plastic strain.[49] The sensitivity of strain rate to stress is mainly determined by the ΔG term. The thermal activation volume (V^*) is expressed by the partial derivative of ΔG with respect to stress, σ.[50] In the present work, V^* is approximated as

$$V^* \equiv k_B T \left.\frac{\partial \ln \dot{\varepsilon}}{\partial \sigma}\right|_{\varepsilon,T} \qquad (7)$$

The derivatives are taken at fixed strain at each temperature to constrain the influence of structure change due to work hardening and softening. Figure 9 plots the thermal activation volume calculated in this case as a function of temperature, peak indentation load, and length scale. As shown, thermal activation volume increases with increase in the length scale of measurements. Since, the thermal activation volume is directly correlated to the deformation energy, the trend implies a significantly high deformation work required at the microscale in comparison to the nanoscale. An almost linear increase in activation volume with increase in temperature implies that deformation mechanism is primarily controlled by dislocations. At the nanoscale the thermal activation volume is 10 times less than that at the microscale indicating that the dislocation pile up is restricted as well as that dislocation climb and diffusion is the main deformation mechanism. At microscale significantly higher thermal activation volume indicates availability of excess free volume in the material structure that can be eliminated by densification. A combination of earlier findings with this result indicates that with increase in length scale the deformation mechanism switches from dislocation diffusion to dislocation pileup. With increase in length scale, dislocation motion does not face significant obstacles or phase transformation related factors. Such factors, if present, will change the almost linear trend observed in Figure 9. The observed trend of the data on peak indentation load as well as stress exponent values at room temperature are in close agreement with the work of Li and Ngan.[15] However, stress exponents are lower than those reported by Li and Ngan for fused silica, indicating a difference in deformation mechanism. The deformation mechanism is intricately linked with the microstructure of this material. The material has $TiSi_2$ particles with higher melting point embedded in SiCO matrix with lower melting point. With increase in temperature, softening of the matrix, particle sliding, and particle rearrangement contribute to deformation mechanism. The effect of these factors is more pronounced at microscale due to higher surface area sampled.

ACKNOWLEDGEMENTS

The authors would like to acknowledge support from US-AFoSR program FA9550-09-1-063 (Program Manager Dr. Ali Sayir), Department of Energy-NETL Program DE-FE0003892, and Department of Energy-NEUP program for supporting various parts of the pre-

sented research work.

References

1. W. Blum and P. Eisenlohr, *Materials Science and Engineering: A,* 510-511 (2009), pp. 7–13.
2. F.H. Norton, *The Creep of Steel at High Temperatures* (New York: McGraw-Hill Book Company, Inc., 1929).
3. R.L. Coble, *J. Applied Physics,* 34 (6) (1963), pp. 1679–1682.
4. C. Herring, *J. Applied Physics,* 21 (5) (1950), pp. 437–445.
5. T.G. Langdon, *Zeitschrift fuer Metallkunde/Materials Research and Advanced Techniques,* 96 (6) (2005), pp. 522–531.
6. J. Harper and J.E. Dorn, *Acta Metallurgica,* 5 (11) (1957), pp. 654–665.
7. J. Weertman, *ASM Transactions Quarterly,* 61 (4) (1968), pp. 681–694.
8. W.D. Nix and B. Ilschner, in *Proc. 5th Int. Conf. on the Strength of Metals and Alloys (ICSMA 5)* (Oxford: Pergamon Press, 1980), pp. 1503–1530.
9. M.E. Kassner and M.T. Perez-Prado, *Progress in Materials Science,* 45 (1) (2000), pp. 1–102.
10. O.D. Sherby and P.M. Burke, *Prog. Mater. Sci.,* 13 (1968), pp. 323–390.
11. W.B. Li, J.L. Henshall, R.M. Hooper, and K.E. Easterling, *Acta Metallurgia et. Materialia,* 39 (12) (1991), pp. 3099–3110.
12. G. Feng and A.H.W. Ngan, *Scripta Materialia,* 45 (8) (2001), pp. 971–976.
13. S.A.S. Asif and J.B. Pethica, *Nanoindentation Creep of Single-Crystal Tungsten and Gallium Arsenide* (London: Taylor & Francis, 1997), pp. 1105–1118.
14. T. Chudoba and F. Richter, *Surface and Coatings Technology,* 148 (2-3) (2001), pp. 191–198.
15. H. Li and A.H.W. Ngan, *J. Materials Research,* 19 (2) (2004), pp. 513–522.
16. J.C.M. Li, K.H.J. Buschow, W.C. Robert, C.F. Merton, I. Bernard, J.K. Edward, M. Subhash, and V. Patrick, *Creep by Indentation*, in *Encyclopedia of Materials: Science and Technology* (Waltham, MA: Elsevier, 2001), pp. 1765–1767.
17. Z.H. Cao, P.Y. Li, H.M. Lu, Y.L. Huang, Y.C. Zhou, and X.K. Meng, *Scripta Materialia,* 60 (6) (2009), pp. 415–418.
18. M.J. Mayo and W.D. Nix, *Acta Metallurgica,* 36 (8) (1988), pp. 2183–2192.
19. B. Lucas and W. Oliver, *Metallurgical and Materials Transactions A,* 30 (3) (1999), pp. 601–610.
20. Z. Zong and W. Soboyejo, *Materials Science and Engineering: A,* 404 (1-2) (2005), pp. 281–290.
21. K. Durst, M. Goken, and G.M. Pharr, *J. Physics D: Applied Physics,* 41 (7) (2008), p. 074005.
22. K. Durst, B. Backes, O. Franke, and M. Göken, *Acta Materialia,* 54 (9) (2006), pp. 2547–2555.
23. H. Li and A.H.W. Ngan, *Scripta Materialia,* 52 (9) (2005), pp. 827–831.
24. V. Jan, F. Dorcakova, J. Dusza, and M. Bartsch, *J. European Ceramic Society,* 28 (1) (2008), pp. 241–246.
25. G. Chollon, J.M. Vallerot, D. Helary, and S. Jouannigot, *J. European Ceramic Society,* 27 (2-3) (2007), pp. 1503–1511.
26. N. Janakiraman and F. Aldinger, *J. Am. Ceram. Soc.,* 93 (3) (2010), pp. 821–829.
27. N. Janakiraman and F. Aldinger, *J. Eur. Ceram. Soc.,* 30 (3) (2010), pp. 775–785.
28. J. Olbricht, A. Yawny, M.L. Young, and G. Eggeler, *Materials Science and Engineering: A,* 510-511 (2009), pp. 407–412.
29. K.B. Khan, T.R.G. Kutty, and M.K. Surappa, *Materials Science and Engineering: A,* 427 (1-2) (2006), pp. 76–82.
30. X. Ma and F. Yoshida, *Applied Physics Letters,* 82 (2) (2003), pp. 188–190.
31. G. Cseh, "Indentation Creep for The Investigation of High Temperature Plastic Behaviour" (Ph.D. thesis, Department of General Physics, Eötvös Loránd University, 2000.
32. A.F. Bower, N.A. Fleck, A. Needleman, and N. Ogbonna, *Proceedings of the Royal Society of London. Series A: Mathematical and Physical Sciences,* 441 (1911) (1993), pp. 97–124.
33. *Investigation of Creep Behaviour using Micro or Nano Indentation Tester (MHT/NHT)* (Needham, MA: CSM Instruments, 2006).
34. Y.T. Cheng and C.M. Cheng, *J. Applied Physics,* 84 (3) (1998), pp. 1284–1291.
35. Z. Zong, J. Lou, O.O. Adewoye, A.A. Elmustafa, F. Hammad, and W.O. Soboyejo, *Materials and Manufacturing Processes,* 22 (2) (2007), pp. 228–237.
36. L. Min and C. Weimin, *Chinese Journal of Aeronautics,* 22 (1) (2009), pp. 43–48.
37. G.J. Fan, H. Choo, P.K. Liaw, and E.J. Lavernia, *Acta Materialia,* 54 (7) (2006), pp. 1759–1766.
38. Y.M. Wang, A.M. Hodge, P.M. Bythrow, J.T.W. Barbee, and A.V. Hamza, *Applied Physics Letters,* 89 (8) (2006), p. 081903-3.
39. R.C. Picu, G. Vincze, F. Ozturk, J.J. Gracio, F. Barlat, and A.M. Maniatty, *Materials Science and Engineering A,* 390 (1-2) (2005), pp. 334–343.
40. E.T. Lilleodden and W.D. Nix, *Acta Materialia,* 54 (6) (2006), pp. 1583–1593.
41. Y.L. Chiu and A.H.W. Ngan, *Acta Materialia,* 50 (6) (2002), pp. 1599–1611.
42. Z.F. Yue, G. Eggeler, and B. Stockhert, *Computational Materials Science,* 21 (1) (2001), pp. 37–56.
43. B. Xu, A. Yonezu, Z. Yue, and X. Chen, *Computational Materials Science,* 46 (2) (2009), pp. 275–285.
44. T. Hidenari, M. Dao, and M. Fujiwara, *J. Physics: Conference Series,* 240 (1) (2010), p. 012004.
45. M. Gan and V. Tomar, *Materials Science and Engineering-A,* 527 (2010), pp. 7615–7623.
46. A.I. Medved' and A.E. Bryukhanov, *Metal Science and Heat Treatment,* 11 (9) (2004), pp. 706–708.
47. Y.-T. Cheng and C.-M. Cheng, *Materials Science and Engineering: R: Reports,* 44 (4-5) (2004), pp. 91–149.
48. J.W. Christian, *The Theory of Transformations in Metals and Alloys* (Oxford, U.K.: Pergamon Press, 1975), p. 81.
49. M.F. Ashby, and H.J. Frost, *Constitutive Equations in Plasticity*, ed. A.S. Argon (Cambridge, MA: MIT Press, 1975), p. 119.
50. J.B. Puthoff, J.E. Jakes, H. Cao, and D.S. Stone, *J. Materials Research,* 24 (3) (2009), pp. 1279–1290.

Ming Gan, Ph.D. candidate, and Vikas Tomar, Associate Professor, are with the Aeronautics and Astronautics Department, Purdue University, West Lafayette, IN, 47906, USA. Dr. Tomar can be reached at (765) 494-3423; e-mail: tomar@purdue.edu.